

# SUSY-QCD corrections to neutralino pair production in association with a jet

Gavin Cullen<sup>1,a</sup>, Nicolas Greiner<sup>2,b</sup>, Gudrun Heinrich<sup>2,c</sup>

<sup>1</sup>Deutsches Elektronen-Synchrotron DESY, Zeuthen, Germany

<sup>2</sup>Max-Planck-Institut für Physik, München, Germany

Received: 16 January 2013 / Revised: 19 March 2013 / Published online: 5 April 2013

© Springer-Verlag Berlin Heidelberg and Società Italiana di Fisica 2013

**Abstract** We present the NLO SUSY-QCD corrections to the production of a pair of the lightest neutralinos plus one jet at the LHC, appearing as a monojet signature in combination with missing energy. We fully include all non-resonant diagrams, i.e. we do not assume that production and decay factorise. We derive a parameter point based on the p19MSSM which is compatible with current experimental bounds and show distributions based on missing transverse energy and jet observables. Our results are produced with the program GOSAM Cullen et al. (Eur. Phys. J. C 72:1889, 2012) for automated one-loop calculations in combination with MadDipole/MadGraph for the real radiation part.

## 1 Introduction

With the LHC experiments performing extremely well, we have entered the exciting phase where we can investigate the properties of a new discovery [2, 3], and get exclusion bounds and hopefully also hints for Beyond the Standard Model physics at energy ranges which have never been probed before.

If the new boson with a mass around 125 GeV is a fundamental scalar, we have to figure out why it is protected from higher order corrections of the order of the Planck scale. Supersymmetry (for a review see e.g. [4, 5] and references therein) offers an elegant explanation for a stabilisation mechanism, and in addition contains massive weakly interacting particles which can serve as dark matter candidates.

While the hopes of an early SUSY discovery at the LHC have withered as recent LHC measurements have pushed

up the lower limits on squark and gluino masses considerably [6–11], there is no stringent lower limit on the mass of the lightest neutralino [12, 13], and the pair production of charginos/neutralinos becomes increasingly important as a “discovery channel” of supersymmetry.

In many SUSY scenarios, the neutralino  $\tilde{\chi}_1^0$  is assumed to be the lightest supersymmetric particle (LSP) and thus is stable if R-parity is conserved. Therefore,  $\tilde{\chi}_1^0 \tilde{\chi}_1^0$  production, either directly or through the decay of heavier neutralinos/charginos, leading to signatures of missing energy and energetic jets/leptons, is a process of primary interest in the context of current SUSY searches. Hence it is desirable to have predictions which include the NLO SUSY-QCD corrections to such processes, not only at the level of total cross sections, but also for differential distributions. While neutralino pair production without any additional jets is not very illuminating from an experimental point of view, the production of neutralino pairs in association with additional jets is interesting, since the signature “missing energy + jets” smells like New Physics, and the distributions of jet observables can be used to investigate the nature (e.g. the spin) of the object(s) carrying away the missing energy.

A very clean signal of new physics would be the observation of an excess in events involving a very energetic monojet in combination with missing transverse energy. Searches for monojets at the LHC at 7 and 8 TeV have been carried out already [14–17], and turned mainly into limits on models involving extra dimensions, assuming that the missing energy is due to graviton production. If the missing energy is due to neutralinos, studying such processes could provide information on the nature and couplings of the LSP and thus on dark matter [18, 19]. Further, monojet signatures are interesting in the context of constraints on invisible decays of the Higgs boson, as the invisibly decaying boson may recoil against hard QCD radiation [20–22].

Total cross sections for the production of charginos and neutralinos at next-to-leading order in QCD have been cal-

<sup>a</sup>e-mail: [gavin.cullen@desy.de](mailto:gavin.cullen@desy.de)

<sup>b</sup>e-mail: [greiner@mpp.mpg.de](mailto:greiner@mpp.mpg.de)

<sup>c</sup>e-mail: [gudrun@mpp.mpg.de](mailto:gudrun@mpp.mpg.de)

culated in [23]. Recently, updates for the LHC at 7 and 8 TeV and current popular benchmark points [24] have been given in [25, 26]. Resummation of large logarithms in the threshold and small- $p_T$  regions has also been carried out [27–29] for the production of gaugino pairs. However, predictions for neutralino pair production in association with one or several jets in a differential form were, until recently, only available at leading order [18]. The first differential NLO QCD corrections for the final state of missing transverse energy in association with two jets, where the missing energy stems from the decay of a squark pair into quarks and neutralinos, have been calculated in [30]. For the case of squark and gluino pair production without decay or additional jets, the number of available results beyond the leading order is larger than for charginos/neutralinos, because these processes were hoped to be seen already at the Tevatron or at early stages of LHC measurements. The first NLO calculations [31–34], partly entering the code `Prospino` [35], were followed by electro-weak corrections [36–40], resummation [41–46] and NNLO threshold corrections [47, 48]. NLO QCD corrections to squark and gluino pair production compared to results from LO matrix element plus parton shower merging have been presented recently in [49], based on calculations in [50, 51].

Next-to-leading order predictions involving chargino or neutralino pairs used in experimental analysis were usually obtained by calculating the NLO K-factors for the total cross sections using e.g. the code `Prospino` [33, 35], and rescaling the LO predictions accordingly. However, it is not at all guaranteed that the same K-factors can be applied globally, in particular in the presence of stringent search cuts. QCD radiation can change the shape of the distributions and affect the mass and spin measurements considerably [52]. If the supersymmetric spectrum is highly compressed, QCD radiation can also seriously affect the exclusion bounds extracted on the basis of leading order assumptions [21, 53].

In this paper, we calculate the NLO QCD corrections to the production of a pair of the lightest neutralinos in association with one jet. We include not only resonant contributions from squark decay, but also all non-resonant contributions. We present our results in a fully differential form, showing distributions for observables involving the jet and missing energy, which can be compared straightforwardly to data. The treatment of diagrams involving resonant squarks needs special attention, as the NLO real corrections formally also contain diagrams which can be regarded as leading order contributions to a different process, which is resonant squark pair production and subsequent decay. We also calculate contributions from Higgs production through a heavy quark or squark loop. However, these contributions are found to be numerically very small. For our studies we consider the phenomenological MSSM (pMSSM) [24, 54, 55], in a variant involving 19 free parameters (p19MSSM). In this framework, we derive a point where the mass of the lightest Higgs

boson  $h$  is  $m_h = 125.8$  GeV. The virtual corrections have been calculated with the automated one-loop program `GOSAM` [1], where the integrals involving complex masses have been called from the integral libraries `Golem95` [56, 57] and `OneLoop` [58]. The real radiation matrix elements are generated using `MadGraph` [59] and `MadDipole` [60, 61].

The paper is organised as follows. In Sect. 2, we describe our method for the calculation of the virtual and real corrections, in particular the generation of the renormalisation counterterms and the treatment of resonant squarks, the latter being further discussed in the Appendix. We also include a phenomenological discussion of MSSM parameter points. In Sect. 3 we present our numerical results, before we conclude in Sect. 4.

## 2 Computational framework

### 2.1 Virtual corrections

The one-loop virtual contribution to the NLO result is calculated using the program `GOSAM` [1]. We use `FeynRules` [62] to produce a model file in the `UFO` [63] format that can be read directly by `GOSAM`.

For the virtual amplitude we have  $\mathcal{O}(1400)$  diagrams to calculate for each subprocess. We neglect  $b$ -quarks in the initial state. The most complicated diagrams are rank-3 pentagons, with up to four internal masses. We illustrate two of the pentagon diagrams in Fig. 1. We include finite widths in the loop integrals and therefore we need a basis set of complex integrals, which we call from the libraries `Golem95C` [57] and `OneLoop` [58]. In general, the consistent introduction of complex masses can induce spurious complex terms in the coupling parameters, as for example in the weak mixing angle. However, the spurious terms in this case are of order  $\mathcal{O}(\frac{\Gamma_W}{M_W}) = \mathcal{O}(\alpha)$  relative to the lowest-order. As the squarks decay weakly to the neutralinos, the effect is also of order  $\alpha$  and therefore can be neglected in the present calculation, as we are only interested in the QCD corrections.

To calculate the loop amplitude in a numerically robust way, `GOSAM` is able to interchange between different reduction schemes at runtime. Our default reduction strategy

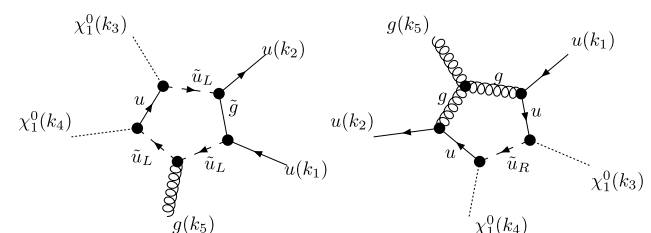


**Fig. 1** Two illustrative pentagon diagrams calculated by `GOSAM`

is to use SAMURAI [64] and, if it fails, to reprocess the point with `Go1em95C` [57] using tensorial reconstruction at integrand level [65]. Due to the large internal masses and the small squark widths present in the integrals, and due to the high rank of the pentagons, numerical stability is a non-trivial issue in this process. Therefore it is crucial that we have this rescue system available during the numerical integration. We use the dimensional reduction scheme (DRED) where only the internal momenta are kept in  $D$  dimensions. We also calculate contributions where neutral Higgs bosons can be produced by a loop-induced process. These can then decay to a pair of the lightest neutralinos.

## 2.2 Counter term diagrams

Due to the appearance of self-energy insertions that can have internal masses different from the mass of the incoming particle we modified the handling of counterterm diagrams from the default GOSAM template file. In the default GOSAM template file each self-energy insertion in the virtual diagrams is rewritten as a sum of the original part plus a part that integrates to give the counterterm diagram. Here we pursue a different approach as follows: each diagram containing a self-energy insertion is “tagged” when the diagram topologies are analyzed. This information is passed through the processing of the diagrams and is available when the numerators of the diagrams are reduced. The counterterm diagram is then reconstructed from the original diagram, by shrinking the self-energy insertions to a point. This is then reduced alongside the loop diagram and written to a separate file for numerical evaluation. The counterterm diagrams depend on model dependent renormalisation constants that we calculate separately. It is planned that this approach will be incorporated into a future release of GOSAM. We use the  $\overline{DR}$  renormalisation scheme, supplemented by on-shell subtraction for the massive particles. As we neglect the masses of the quarks of the first two generations, we do not need any renormalisation of the mixing angle. The renormalisation of the squark sector is outlined in more detail in Appendix C.

## 2.3 Real corrections and numerical integration

The leading order (LO) and the real radiation matrix elements are generated using `MadGraph` [59]. For the subtraction of the infrared singularities we use Catani–Seymour dipoles [66], supplemented with a phase space restriction parameter  $\alpha$  as proposed in [67] and implemented in the package `MadDipole` [60, 61]. The generation of the various pieces of the code (tree-level, real emission process, subtraction terms) and their combination with the integration routines was performed in a fully automated way. For the numerical integration we used `MadEvent` [68, 69], slightly modified in order to integrate the different NLO contributions.

## 2.4 Treatment of diagrams with resonant squarks

For processes involving unstable particles, the proper definition of the set of diagrams contributing to the next-to-leading order corrections is not obvious. There are problems of double counting as diagrams with additional real radiation from the unstable particle in the final state can, if it becomes resonant, also be regarded as part of a leading order process with the decay already included in the narrow width approximation. The problem is similar to the case of  $Wt$  and  $W^+W^-b\bar{b}$  production at NLO, where the  $W^+W^-b\bar{b}$  final state occurring in the NLO real corrections, if stemming from doubly resonant top decays, can also be viewed as belonging to leading order  $t\bar{t}$  production and decay. This problem has been discussed in detail in [70, 71] for the case of  $Wt$  production. The case at hand is very similar, with  $t \rightarrow Wb$  replaced by  $\tilde{q} \rightarrow \tilde{\chi}_1^0 q$ . Consider for example the leading order diagrams in Fig. 2. Squark exchange in the t-channel, as shown in Fig. 2(a), cannot lead to any resonance, but in the case of s-channel squark exchange shown in Fig. 2(b), the squark can become resonant, and it can be viewed as a diagram for squark production in association with a neutralino, with squark decay included in the narrow width approximation. Now at NLO, when the real radiation of an additional parton is included, a new channel opens up, where two squarks can decay resonantly into a quark and a neutralino, as shown in Fig. 3. Close to the resonance, this contribution gets quite large, and in fact should rather be counted as a leading order contribution to squark pair production with subsequent squark decay, because here we are interested in the radiative corrections to the final state of a monojet in association with a neutralino pair.

For this reason the calculation was carried out in two different ways. In the first approach we take into account all possible diagrams leading to the required final state consisting of two neutralinos and two QCD partons. In particular this includes the possibility of having two on-shell squarks.

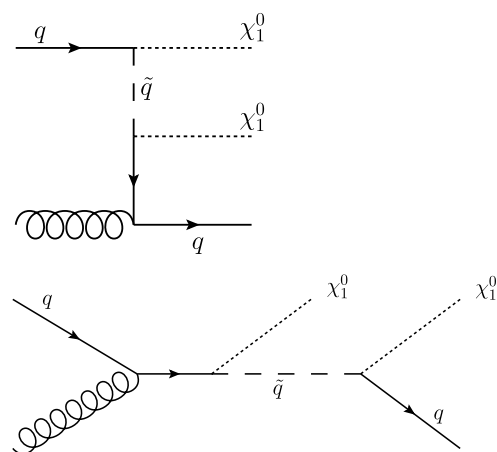


**Fig. 2** Examples of a leading order diagrams with a squark in (a) the t-channel, (b) the s-channel

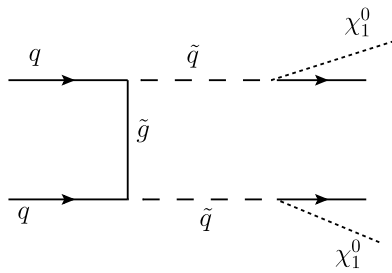


**Fig. 3** Example of a “doubly resonant” squark diagram occurring in the NLO real corrections

As it turns out, the real radiation part is vastly dominated by these diagrams, spoiling the convergence of the perturbation series. The result behaves like a tree-level calculation, involving one more order in the strong coupling constant than the tree level for the monojet case. The difference from an actual tree-level calculation is given by the fact that one parton can become unresolved, leading to the signal “single jet plus missing energy”, while the infrared singularities due to the unresolved parton are cancelled by the virtual corrections or absorbed into the parton distribution functions. Therefore, even though the calculation which includes these resonant diagrams cannot be regarded as a genuine next-to-leading order correction to the cross section describing a neutralino pair in association with one jet, it is still a physically meaningful quantity. However, from an experimental point of view, a complete description of the final state of missing energy plus up to two jets would be more useful. This, however, would require the full NLO calculation of the production of a neutralino pair in association with two jets, where the jets can either originate from the decay of squarks and gluinos or be produced directly from partons in the hard interaction. This is a very complex task which is beyond the scope of this paper.

In the second approach we follow a strategy proposed in [70], namely we remove the diagrams with two squarks in the s-channel from the amplitude. Removing diagrams from the amplitude generally violates gauge invariance. Reference [70] contains a study about the impact of violating gauge invariance by such a removal of diagrams, where the effects were found to be small for commonly used gauges.

For our calculation we assume that the largest contribution of diagrams with two squarks in the s-channel come from those points in phase space where both squarks are on-shell, and that off-shell effects are suppressed by a factor of  $\Gamma/M$ . Therefore it is sufficient to consider the  $2 \rightarrow 2$  process of producing two squarks. In this case one can show that the gauge dependence vanishes for covariant gauges and for a large class of non-covariant gauges. We give a proof in Appendix B.

Another solution to the double counting problem based on the subtraction of the resonant diagrams is the so-called

“prospino scheme” [33, 51], where in its most recent variant [49] a subtraction term is introduced which involves a momentum remapping oriented at Catani–Seymour mappings to preserve the on-shell conditions for both intermediate and final state momenta. The subtraction term is then constructed in such a way that it comes into operation when the intermediate particle goes on-shell. However, for multiparticle final states where the Born process is already  $2 \rightarrow 3$  or of higher multiplicity, and doubly resonant diagrams appear at NLO, the generalisation of this procedure is not obvious.

## 2.5 Phenomenological discussion of SUSY parameter points

The discovery of a boson with mass of about 125 GeV [2, 3] and a lack of any experimental evidence for supersymmetry has put many SUSY models under strain. In particular, the family of the so-called constrained MSSM (cMSSM) is increasingly unfavoured in light of the present experimental data [72, 73]. Therefore we choose a more pragmatic and experimentally motivated parameterisation of SUSY, known as the phenomenological MSSM (pMSSM) [24, 54, 55], in a variant involving 19 free parameters (p19MSSM). In the pMSSM, no underlying SUSY breaking scenario is chosen, and gauge coupling unification is not postulated. However, it is assumed that there are no sources of CP violation and generation mixing beyond the Standard Model ones, so that all off-diagonal elements in the sfermion mass matrices are equal to zero, and the first and second-generation soft terms are equal. We will further assume that the LSP is the lightest neutralino.

In such models we can corner the parameter space where the squarks, gluino, and neutralinos have masses close together. This region is of particular interest for the process considered here, as the squark masses can be low enough for the signal to be significant at LHC energies while evading the current LHC exclusion regions.

Compressed spectra of this type were also studied in [12, 21, 53] where the search for SUSY through the recoil of light SUSY particles against initial state radiation is discussed. Our choice of SUSY parameter point can be viewed as qualitatively like the “Equal Mass” scenario in Ref. [53]. In this situation we expect to see soft jets from the decays of the squarks to the neutralino.

For our results we choose a modification of the parameter point p19MSSM1.1 which we call the p19MSSM1Amod. The p19MSSM1 line was introduced in [24] and was constructed as a benchmark for these compressed SUSY scenarios, and is labelled by an integer  $N$ , i.e. p19MSSM1. $N$ . The p19MSSM1 line is controlled by one parameter: the gaugino mass parameter  $M_1$ . The two lightest generation sfermion masses  $M_{\tilde{f}_{1,2}}$  and the mass of the gluino,  $M_3$ , are fixed at

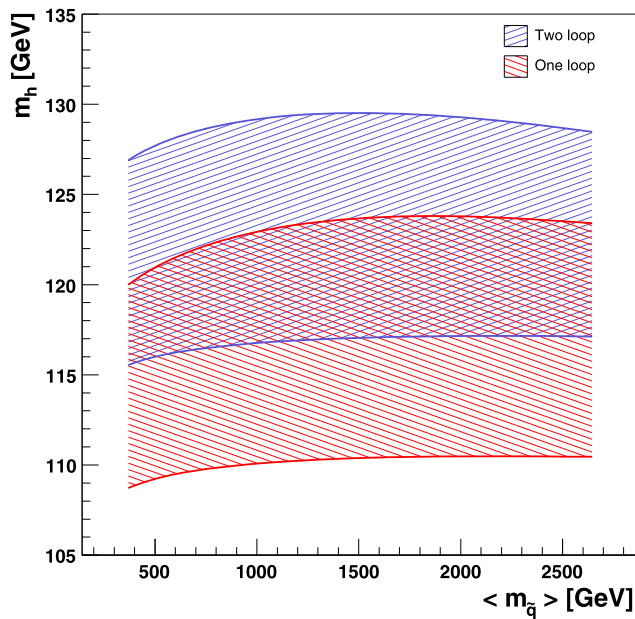


**Fig. 4** The lightest Higgs boson in the MSSM depends on the parameter  $A_t$  through one-loop and two-loop corrections. Here, the band illustrates how  $m_h$  varies with  $A_t$  in the benchmark scenario p19MSSM1. This variation is examined over a range of input parameters  $M_1$  which changes the spectrum of the light squark masses. The  $x$ -axis is the average value of the light squark masses

$1.2M_1$ . p19MSSM1. $N$  is defined for  $N = 1$  at the value  $M_1 = 300$  GeV and this is increased by 100 GeV for each subsequent value of  $N$ . We effectively decouple all other particles in the model by setting the other mass parameters to a higher scale, here 2500 GeV. We choose a value of 10 for  $\tan\beta$ .

Our choice modifies p19MSSM1.1 in two ways. Firstly, we make contact with the point p19MSSM1A, given in [30], by setting the heavier Higgs bosons mass inputs,  $\mu$  and  $m_A$ , to the higher scale. Like the heavier squarks these particles are effectively decoupled. Secondly, we further modify this point by choosing  $A_t = 5000$  such that the mass of the lightest Higgs  $h$  in our model can be identified with the boson observed at the LHC with mass  $m_h = 125.8$  GeV. We illustrate the effect that varying  $A_t$  has on the mass of the lightest Higgs boson from  $A_t = 0$  to the maximum Higgs mass in Fig. 4 over a range of the gaugino mass parameter  $M_1$ . We do not plot the theory uncertainty coming from unknown higher order corrections nor the uncertainty from the input parameters. The SUSY masses that we use for our calculation, at this point in parameter space, are given explicitly in Table 2.

The particle spectrum was produced using SOFTSUSY [74] and then the decay widths calculated using the package SUSYHIT [75] in which we used the packages HDECAY [76] and SDECAY [77]. GOSAM can read input cards provided in the SLHA format [78, 79] allowing one to

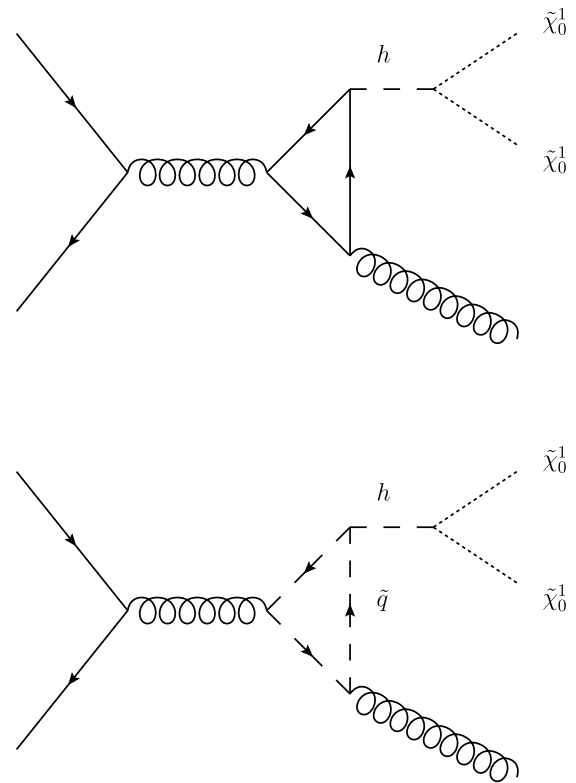


**Fig. 5** Examples of a loop diagrams involving the MSSM Higgs bosons. Here  $h$  stands for any of the MSSM Higgs bosons in the set  $\{h, H, A\}$

change the SUSY parameter point without recompiling the code.

### 2.6 Higgs contribution to the signal

As mentioned in Sect. 2.1 we also calculate the contribution arising from Higgs production through heavy quark and squark loops with subsequent Higgs decay to a neutralino pair.

We illustrate these types of diagram in Fig. 5. To quantify their contribution to the total cross section we can easily isolate these types of diagrams using the diagram filtering system in GOSAM. We find the Higgs boson contribution to the total cross section to be negligible, so these diagrams are not included in the results shown in Sect. 3.

### 2.7 Checks on the result

We have checked that after UV renormalisation, all poles from the virtual contributions cancel with the poles from the infrared insertion operator [66] in the real radiation. We have also checked the unrenormalised virtual matrix element against the program FeynArts/FormCalc [80–82]. We found agreement for the partonic subprocess  $ug \rightarrow \chi_1^0 \chi_1^0 u$ . All other subprocesses can be found by exploiting crossing symmetry.

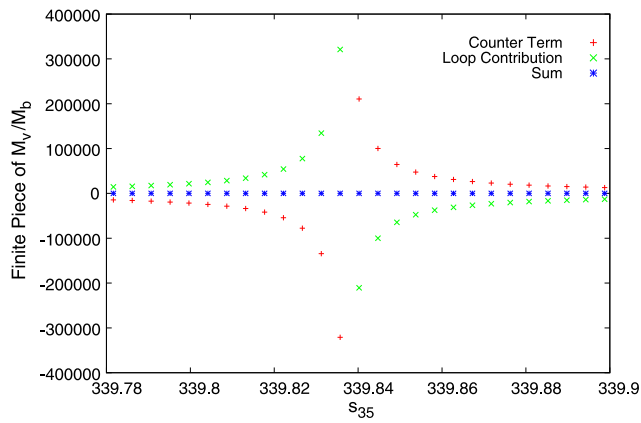


**Fig. 6** Cancellation of the finite remainders of the UV divergent parts of the amplitude with the corresponding counterterms in the resonance region

Furthermore, we checked our renormalisation procedure by investigating the cancellation of the finite remainders of the UV divergent loop contributions with the counterterms, as illustrated in Fig. 6.

### 3 Phenomenological results

In this section we present a selection of phenomenological results for proton–proton collisions at the LHC at 8 TeV.

#### 3.1 Setup and cuts

For all the results and distributions shown in this section we have used the parameters listed in Tables 1 and 2.

The weak mixing angle is calculated from the  $W$  and  $Z$  masses. The strong coupling constant and its running are determined by the set of parton distribution functions. We used an NLO pdf set from NNPDF2.3 [83], where the values for  $\alpha_s$  at leading order and next-to-leading order are given by

$$\alpha_s(M_Z) = 0.119,$$

and the running is calculated at one loop for the tree-level result and at two loops for the next-to-leading order parts. As we neglect initial state  $b$ -quarks, we use the  $N_f = 4$  version of the pdf set. Further, we assume flavour-diagonal SUSY-QCD couplings.

**Table 1** Standard Model parameters used for the phenomenological study

Standard model parameters	
$M_Z = 91.188$ GeV	$\Gamma_Z = 2.4952$ GeV
$M_t = 173.4$ GeV	$\Gamma_t = 1.4384$ GeV
$\alpha(M_Z) = 1/127.934$	

**Table 2** Masses and widths of the supersymmetric particles for the benchmark point used. The second generation of squarks is degenerate with the first generation of squarks. All parameters are given in GeV

SUSY parameters	
$M_{\tilde{\chi}_1^0} = 299.5$	$\Gamma_{\tilde{\chi}_1^0} = 0$
$M_{\tilde{g}} = 415.9$	$\Gamma_{\tilde{g}} = 4.801$
$M_{\tilde{u}_L} = 339.8$	$\Gamma_{\tilde{u}_L} = 0.002562$
$M_{\tilde{u}_R} = 396.1$	$\Gamma_{\tilde{u}_R} = 0.1696$
$M_{\tilde{d}_L} = 348.3$	$\Gamma_{\tilde{d}_L} = 0.003556$
$M_{\tilde{d}_R} = 392.5$	$\Gamma_{\tilde{d}_R} = 0.04004$
$M_{\tilde{b}_L} = 2518.0$	$\Gamma_{\tilde{b}_L} = 158.1$
$M_{\tilde{b}_R} = 2541.8$	$\Gamma_{\tilde{b}_R} = 161.0$
$M_{\tilde{t}_L} = 2403.7$	$\Gamma_{\tilde{t}_L} = 148.5$
$M_{\tilde{t}_R} = 2668.6$	$\Gamma_{\tilde{t}_R} = 182.9$

For the jet clustering we used an anti- $k_T$  algorithm [84] with a cone size of  $R = 0.4$  provided by the `FastJet` package [85, 86]. We choose  $\mu = H_T/2$  for our central scale, where we define  $H_T$  as  $H_T = \sum_i E_{T,i}$  with  $i$  running over the momenta of the two neutralinos and the jet(s).

We use the following set of cuts:

$$p_T(\text{leading jet}) \geq 100 \text{ GeV}, \quad |\eta_j| \leq 4.5. \quad (1)$$

In addition we impose a cut on the missing transverse energy of

$$E_{T,\text{miss}} \geq 85 \text{ GeV}. \quad (2)$$

We also impose a jet veto of 30 GeV on a second jet which at NLO originates from the  $2 \rightarrow 4$  part of the real radiation corrections, as discussed in Sect. 2.4. Our relatively low cut on the transverse missing energy is motivated by the fact that the neutralinos  $\tilde{\chi}_1^0$  could be rather light, and therefore the requirement of very large  $E_{T,\text{miss}}$ , which is well motivated in searches for graviton production in association with monojets, could be too restrictive in the case of neutralino pair production in association with one jet. In this case the neutralinos do not originate from long cascades of heavier objects with additional missing energy produced along the cascade.

#### 3.2 Numerical results

In this section we show distributions for the observables  $p_T^j$ , the transverse momentum of the jet, the missing transverse energy  $E_T^{\text{miss}}$ , and the angle  $\phi(\mathbf{p}^{\text{miss}}, \mathbf{p}^j)$ , where  $\mathbf{p}^{\text{miss}}$  is defined as minus the vector sum of the visible particles in the event, and  $\mathbf{p}^j$  is the momentum of the leading jet. We show two types of distributions for each observable: one where each distribution is normalised to one in order to exhibit the difference in shape, and another with absolute values. For

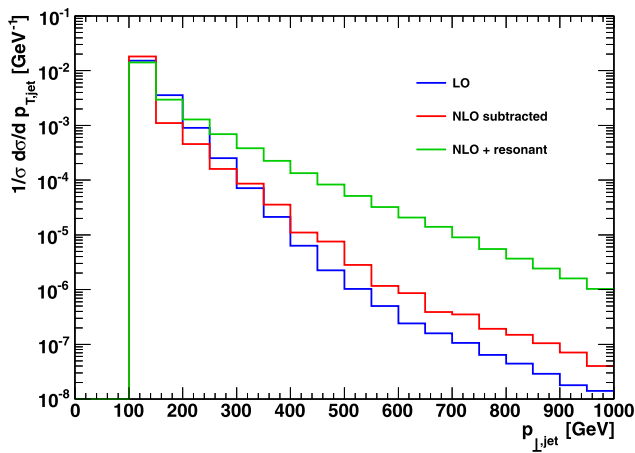


**Fig. 7** Normalised distributions showing the transverse momentum distribution of the leading jet for the process  $pp \rightarrow \tilde{\chi}_1^0 \tilde{\chi}_1^0 + \text{jet}$  at  $\sqrt{s} = 8$  TeV, comparing the cases where the resonant diagrams are included to the ones where they are subtracted

the normalised histograms in Figs. 7, 9 and 11, we show results for both approaches, the one including the doubly resonant diagrams and the one with diagram removal.

Investigating the behaviour of the cross sections under scale variations, we observe the following. As expected, the results including the doubly resonant diagrams show no improvement of the scale uncertainty at NLO, because they are completely dominated by the  $2 \rightarrow 4$  real radiation, and therefore the scale dependence is not compensated by the virtual contributions. The case where these diagrams are removed is still dominated by the new channels opening up in the NLO real radiation contributions. Therefore, in this case we do not find a stabilisation of the scale dependence either. However, the cross sections are sizeable. Using  $\mu = \mu_R = \mu_F$  and varying between  $H_T/4 \leq \mu \leq 2H_T$ , we find 20–30 fb for the LO cross section, while the NLO subtracted cross section amounts to about 100 fb for the central scale, and the one including doubly resonant diagrams to 960 fb for the central scale. This means that the point p19MSSM1Amod considered here could in principle be tested with the data accumulated so far.

For the results including the doubly resonant diagrams, it is pointless to determine a K-factor, as in this case it is not well defined to which leading order process the higher order terms should be attributed, as explained in Sect. 2.4.

For the subtracted case, where we show absolute as well as normalised results, the K-factors are still quite large, as can be seen from Figs. 8, 10 and 12. This can be understood as being mainly due to new channels opening up in the NLO real radiation part, in the presence of an additional QCD parton. The distributions also show that the K-factors are not uniform, which implies that the “standard” procedure to use K-factors based on total cross sections calculated at NLO can be misleading. For the angle  $\phi(\mathbf{p}^{\text{miss}}, \mathbf{p}^j)$  between the

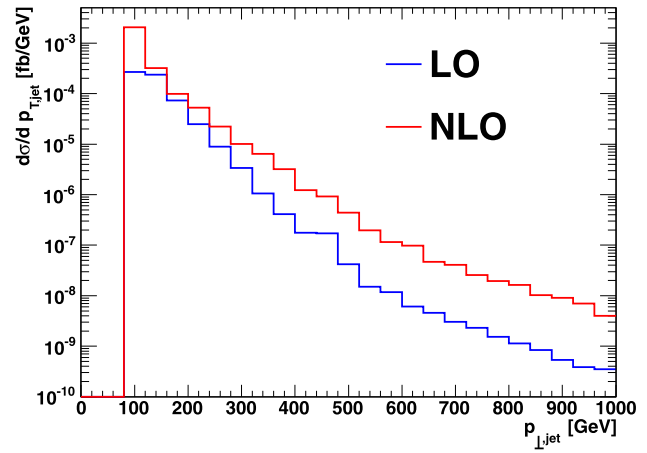


**Fig. 8** Transverse momentum distribution of the leading jet for the process  $pp \rightarrow \tilde{\chi}_1^0 \tilde{\chi}_1^0 + \text{jet}$  at  $\sqrt{s} = 8$  TeV

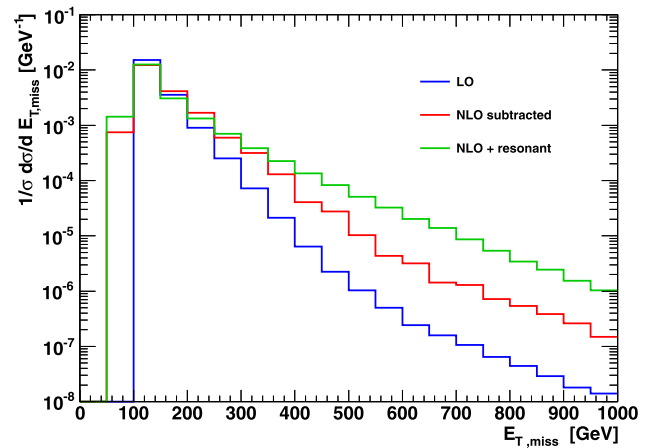


**Fig. 9** Normalised distributions showing the missing transverse energy  $E_T^{\text{miss}}$ , comparing the cases where the resonant diagrams are included to the ones where they are subtracted

jet and the missing momentum, shown in Figs. 11 and 12, NLO is obviously the first order where the fixed order prediction makes sense, because at LO the vector sum of the neutralino momenta will always be back-to-back to the recoiling jet.

The large K-factors can partly be attributed to the fact that at NLO, a considerable number of new partonic channels are opening up: the gluon-gluon initiated processes, and the ones initiated by  $uu, dd, \bar{u}d, u\bar{d}$  are all absent at leading order (where only  $q\bar{q}$  and  $qg/\bar{q}g$  are present) and the new channels together make up almost 50 % of the cross section. If we roughly estimate the K-factor which would result from partonic initial states which are already present at LO, it would amount to  $K \sim 2.3$ . Further, we investigated the point SPS1a [87] just for reference, and found that for this point the K-factors are also smaller. This can be attributed to the fact that for the compressed spectrum we are consider-

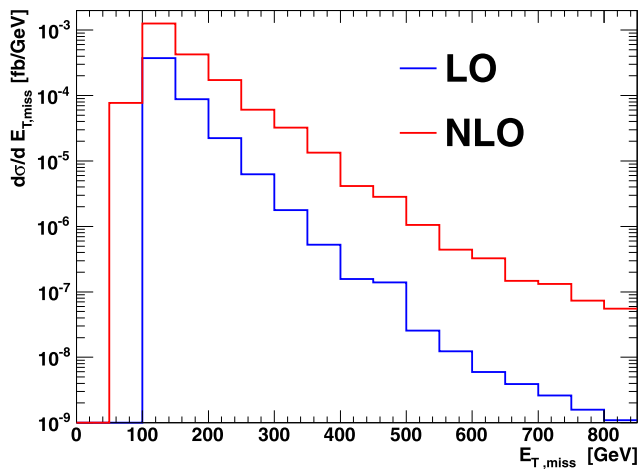


**Fig. 10** Distribution showing the missing transverse energy  $E_T^{\text{miss}}$  for the process  $pp \rightarrow \tilde{\chi}_1^0 \tilde{\chi}_1^0 + \text{jet}$  at  $\sqrt{s} = 8$  TeV

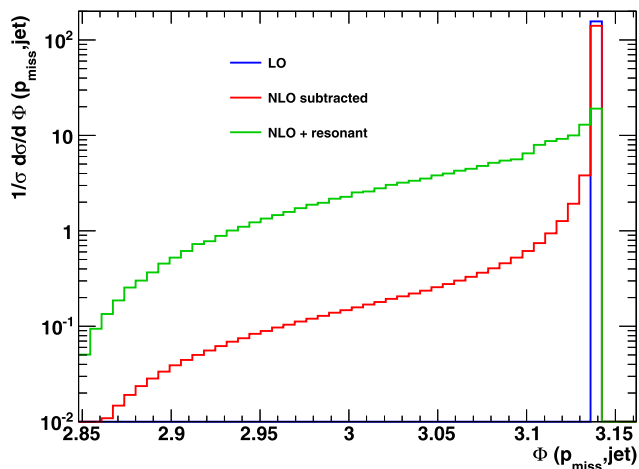


**Fig. 11** Normalised distributions showing the angle  $\phi(\mathbf{p}^{\text{miss}}, \mathbf{p}^j)$ , comparing the cases where the resonant diagrams are included to the ones where they are subtracted

ing here, the widths of the first generation squarks are very small, leading to larger contributions if the squarks are close to being on-shell.

## 4 Conclusions

We have calculated the NLO SUSY-QCD corrections to the production of a pair of the lightest neutralinos in association with one jet. We did not use the approximation of factorising production and decay, but fully included all non-resonant contributions. Contributions from Higgs production through a heavy quark or squark loop were calculated and found to be numerically negligible. The calculation has been performed using two different approaches to treat the doubly resonant diagrams appearing in the NLO real radi-

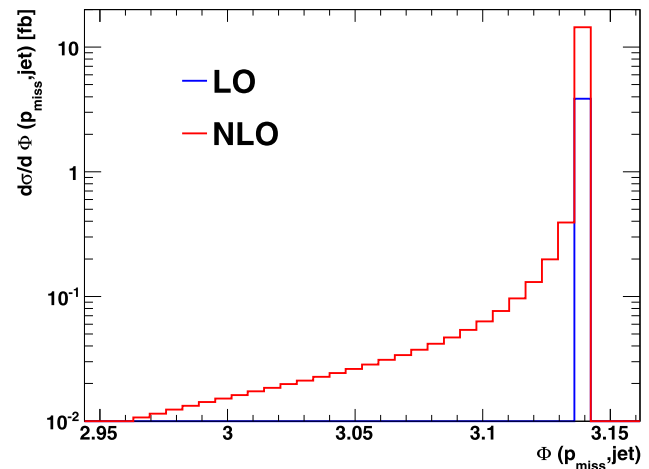


**Fig. 12** The angle  $\phi(\mathbf{p}^{\text{miss}}, \mathbf{p}^j)$  between the leading jet and missing momentum vectors, where the latter is defined as the negation of the visible momenta in the event

tion contribution: one is based on diagram removal and the other based solely on a veto on the second jet. In the latter approach, the K-factors are obviously very large as the whole result is dominated by a reaction which can also be viewed as the Born level for a different process (resonant squark pair production with a subsequent factorisable decay into a neutralino and a jet). We present our results in a fully differential form, based on the experimentally accessible jet and missing  $E_T$  observables.

On a technical level, to the best of our knowledge, this is the first  $2 \rightarrow 3$  NLO calculation within the MSSM which includes full off-shell effects, as well as complex masses. Even though we only consider the phenomenological MSSM (p19MSSM) here, we would like to emphasise that our setup is largely automated, using the public one-loop program GOSAM in combination with MadGraph, MadDipole and FeynRules, such that other parameter points, and even other models Beyond the Standard Model, can be studied as well within the same framework.

**Acknowledgements** We would like to thank Wolfgang Hollik, Jonas Lindert, Edoardo Mirabella, Davide Pagani, and the members of the GoSam collaboration for various useful discussions. We also acknowledge use of the computing resources at the Rechenzentrum Garching. The work of G.C. was supported by DFG Sonderforschungsbereich Transregio 9, Computergestützte Theoretische Teilchenphysik. We also acknowledge the support of the Research Executive Agency (REA) of the European Union under the Grant Agreement number PITN-GA-2010-264564 (LHCPhenoNet).

## Appendix A: Leading order diagrams

In Figs. 13 and 14 we display the 14 diagrams contributing at leading order to the process  $u\bar{u} \rightarrow \tilde{\chi}_1^0 \tilde{\chi}_1^0 g$ . The diagrams for the  $ug \rightarrow \tilde{\chi}_1^0 \tilde{\chi}_1^0 u$  subprocess can be obtained by crossing.

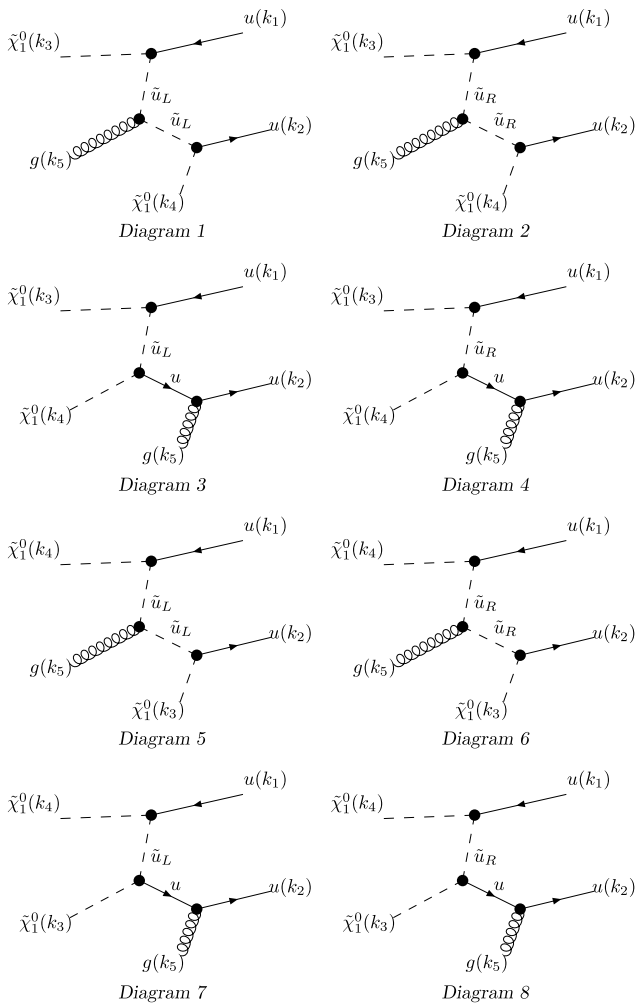


**Fig. 13** Tree level diagrams 1 to 8 for the process  $u\bar{u} \rightarrow \tilde{\chi}_1^0 \tilde{\chi}_1^0 g$

**Appendix B: Gauge dependence**

In this appendix we examine the gauge dependence of the diagrams that have been removed from the amplitude in the real emission part as discussed in Sect. 2.4. We show that this gauge dependence vanishes for covariant gauges and for a large class of non-covariant gauges.

The only diagrams, once omitted, that can lead to a dependence on the choice of gauge are of the type shown in Fig. 15. In this diagram there is an s-channel gluon which decays into a squark–antisquark pair. As the biggest contribution to the cross section comes from the parts of the phase space where the two squarks are on-shell, it is sufficient for our argument to consider the  $2 \rightarrow 2$  process of squark pair production and neglect the subsequent decay of the squarks. We denote the incoming momenta of the quarks as  $q_1, q_2$  and the outgoing momenta of the squarks as  $p_1, p_2$ . In the following we neglect overall prefactors like color factors and coupling constants as they are irrelevant for our argument. The same holds for factors of  $i$  and any minus signs. The

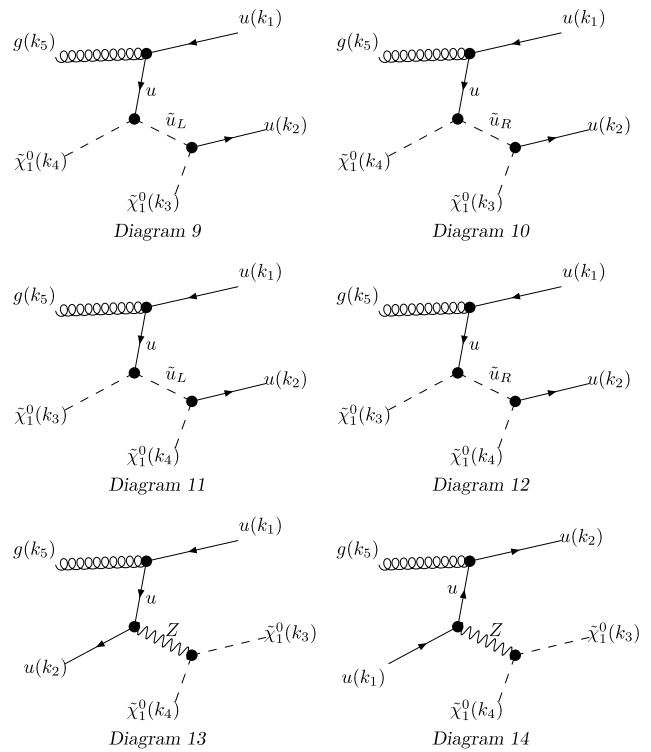


**Fig. 14** Tree level diagrams 9 to 14 for the process  $u\bar{u} \rightarrow \tilde{\chi}_1^0 \tilde{\chi}_1^0 g$

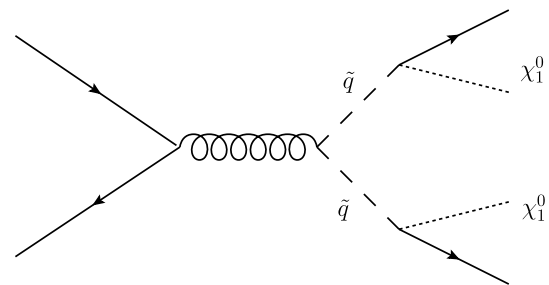


**Fig. 15** Diagram of squark pair production via a s-channel gluon and their subsequent decay

amplitude of the  $2 \rightarrow 2$  process can be written as

$$\mathcal{M} \sim \bar{v}(q_1)\gamma^\mu D_{\mu\nu}u(q_2) \cdot (p_1^\nu - p_2^\nu), \tag{B.1}$$

where  $D_{\mu\nu}$  denotes the gluon propagator, which in Feynman gauge is simply given by

$$D_{\mu\nu} = -\frac{g_{\mu\nu}}{k^2} \quad \text{with } k = q_1 + q_2. \tag{B.2}$$

Choosing the Feynman gauge and contracting the Lorentz indices expression gives

$$\mathcal{M} \sim \bar{v}(q_1)(\not{p}_1 - \not{p}_2)u(q_2) \tag{B.3}$$

and after squaring and performing the fermion spin sum one obtains

$$|\mathcal{M}|^2 \sim \text{tr}(\not{q}_1(\not{p}_1 - \not{p}_2)\not{q}_2(\not{p}_1 - \not{p}_2)). \tag{B.4}$$

As the gluon propagator is gauge dependent, the gauge dependence vanishes only in the sum of all contributing amplitudes.

To calculate the effect of a specific gauge to the given diagram we start with a general covariant gauge. The gluon propagator can be written as

$$D_{\mu\nu} = -\frac{1}{k^2} \left( g_{\mu\nu} + (1 - \lambda) \frac{k_\mu k_\nu}{k^2} \right), \tag{B.5}$$

so that, for  $\lambda = 1$ , we recover the Feynman gauge. In the general case the presence of a term  $k_\mu k_\nu$  leads to an extra term in Eq. (B.3) of the form  $\not{k}(k \cdot p_1 - k \cdot p_2)$ . It can easily be seen that this extra term vanishes if one replaces

$$\not{k} = \not{q}_1 + \not{q}_2 \tag{B.6}$$

and makes use of the Dirac equation for massless quarks,

$$\not{q}_2 u(q_2) = 0, \quad \bar{v}(q_1) \not{q}_1 = 0. \tag{B.7}$$

Next, we turn to the case of non-covariant gauges. We consider the following structure for the gluon propagator:

$$D_{\mu\nu} = -\frac{1}{k^2} \left( g_{\mu\nu} - \frac{n_\mu k_\nu + n_\nu k_\mu}{n \cdot k} + \frac{n^2 k_\mu k_\nu}{(n \cdot k)^2} \right), \tag{B.8}$$

where  $n$  can be a time-like, space-like or light-like vector.

The third term of Eq. (B.8) vanishes with the same argument as for covariant gauges, as well as the term  $\sim n_\nu k_\mu$ .

The remaining term can be written as

$$\not{n}(k \cdot p_1 - k \cdot p_2) = \not{n}(q_1 \cdot p_1 + q_2 \cdot p_1 - q_1 \cdot p_2 - q_2 \cdot p_2). \tag{B.9}$$

Momentum conservation in the on-shell limit implies

$$q_1 \cdot p_1 = q_2 \cdot p_2, \quad q_2 \cdot p_1 = q_1 \cdot p_2, \tag{B.10}$$

and therefore the additional factor in Eq. (B.9) is zero.

### Appendix C: Renormalisation

In this appendix we outline how we perform the renormalisation of the squark mass and wavefunction.

To begin we write the renormalised self-energy as follows:

$$\Sigma^R(s, m_{\tilde{q}}^2 - im_{\tilde{q}}\Gamma_{\tilde{q}})$$

$$= (s - m_{\tilde{q}}^2 + im_{\tilde{q}}\Gamma_{\tilde{q}}) + A(s, m_{\tilde{q}}^2 - im_{\tilde{q}}\Gamma_{\tilde{q}}) + \delta Z_{\tilde{q}}(s - m_{\tilde{q}}^2 + im_{\tilde{q}}\Gamma_{\tilde{q}}) - \delta\mu_{\tilde{q}}^2 + \mathcal{O}(\alpha_s^2), \tag{C.1}$$

where  $A$  is the one-loop contribution to the self-energy. The on-shell renormalisation condition is that the renormalised one-loop self-energy is equal to the inverse of the bare propagator in the limit (up to order  $\alpha_s^2$ ):

$$\lim_{s \rightarrow m_{\tilde{q}}^2 - im_{\tilde{q}}\Gamma_{\tilde{q}}} \Sigma^R(s, m_{\tilde{q}}^2 - im_{\tilde{q}}\Gamma_{\tilde{q}}) = s - m_{\tilde{q}}^2 + im_{\tilde{q}}\Gamma_{\tilde{q}}. \tag{C.2}$$

We expand  $A$ :

$$\begin{aligned} &A(s, m_{\tilde{q}}^2 - im_{\tilde{q}}\Gamma_{\tilde{q}}) \\ &= A(m_{\tilde{q}}^2 - im_{\tilde{q}}\Gamma_{\tilde{q}}, m_{\tilde{q}}^2 - im_{\tilde{q}}\Gamma_{\tilde{q}}) \\ &\quad + (s - m_{\tilde{q}}^2 + im_{\tilde{q}}\Gamma_{\tilde{q}}) A'(m_{\tilde{q}}^2 - im_{\tilde{q}}\Gamma_{\tilde{q}}, m_{\tilde{q}}^2 - im_{\tilde{q}}\Gamma_{\tilde{q}}) \\ &\quad + \mathcal{O}[(s - m_{\tilde{q}}^2 + im_{\tilde{q}}\Gamma_{\tilde{q}})^2] \end{aligned} \tag{C.3}$$

and then (C.2) fixes our renormalisation constants:

$$\begin{aligned} \delta Z_{\tilde{q}} &= -A'(m_{\tilde{q}}^2 - im_{\tilde{q}}\Gamma_{\tilde{q}}, m_{\tilde{q}}^2 - im_{\tilde{q}}\Gamma_{\tilde{q}}), \\ \delta m_{\tilde{q}}^2 &= A(m_{\tilde{q}}^2 - im_{\tilde{q}}\Gamma_{\tilde{q}}, m_{\tilde{q}}^2 - im_{\tilde{q}}\Gamma_{\tilde{q}}). \end{aligned} \tag{C.4}$$

### Appendix D: Expansion around real arguments

To circumvent using scalar integrals with complex incoming momentum we show how one can expand  $A$  around the real mass and end with renormalisation constants that look like the usual ‘real’ case but with complex internal masses. We follow the argument presented in [88].

$$\begin{aligned} &A(m_{\tilde{q}}^2 - im_{\tilde{q}}\Gamma_{\tilde{q}}, m_{\tilde{q}}^2 - im_{\tilde{q}}\Gamma_{\tilde{q}}) \\ &= A(m_{\tilde{q}}^2, m_{\tilde{q}}^2 - im_{\tilde{q}}\Gamma_{\tilde{q}}) \\ &\quad - im_{\tilde{q}}\Gamma_{\tilde{q}} A'(m_{\tilde{q}}^2, m_{\tilde{q}}^2 - im_{\tilde{q}}\Gamma_{\tilde{q}}) + \mathcal{O}((m_{\tilde{q}}\Gamma_{\tilde{q}})^2). \end{aligned} \tag{D.1}$$

We can therefore expand (C.4) to

$$\delta Z_{\tilde{q}} = -A'(m_{\tilde{q}}^2, m_{\tilde{q}}^2 - im_{\tilde{q}}\Gamma_{\tilde{q}}), \tag{D.2}$$

$$\begin{aligned} \delta\mu_{\tilde{q}}^2 &= A(m_{\tilde{q}}^2, m_{\tilde{q}}^2 - im_{\tilde{q}}\Gamma_{\tilde{q}}) - im_{\tilde{q}}\Gamma_{\tilde{q}} A'(m_{\tilde{q}}^2, m_{\tilde{q}}^2 \\ &\quad - im_{\tilde{q}}\Gamma_{\tilde{q}}). \end{aligned} \tag{D.3}$$

Now, if we substitute these into (C.1) we obtain (substituting  $\mu^2 = m_{\tilde{q}}^2 - im_{\tilde{q}}\Gamma_{\tilde{q}}$ ):

$$\begin{aligned} &\Sigma^{R,1}(s, \mu^2) \\ &= A(s, \mu^2) + \delta Z_{\tilde{q}}(s - \mu^2) - \delta\mu_{\tilde{q}}^2 \end{aligned}$$

$$\begin{aligned}
 &= A(s, \mu^2) - A'(m_{\tilde{q}}^2, \mu^2)[(s - \mu^2) + (\mu^2 - m_{\tilde{q}}^2)] \\
 &\quad - A(m_{\tilde{q}}^2, \mu^2) \\
 &= A(s, \mu^2) - A'(m_{\tilde{q}}^2, \mu^2)[s - m_{\tilde{q}}^2] - A(m_{\tilde{q}}^2, \mu^2) \\
 &= A(s, \mu^2) + \delta Z_R(s - m_{\tilde{q}}^2) - \delta m_{\tilde{q}}^2 \tag{D.4}
 \end{aligned}$$

where

$$\delta Z_R = -A'(m_{\tilde{q}}^2, \mu^2), \quad \delta m_{\tilde{q}}^2 = A(m_{\tilde{q}}^2, \mu^2). \tag{D.5}$$

Therefore our expansion looks like the usual real on-shell scheme, but with complex internal masses.

We now list the explicit results for the renormalisation constants. The constant for the mass counterterm is

$$\begin{aligned}
 \delta m_{\tilde{q}}^2 &= \frac{\alpha_s}{4\pi} C_F [-4\mu_{\tilde{q}}^2 I_2^n(m_{\tilde{q}}^2, 0, \mu_{\tilde{q}}^2) + 2\mu_{\tilde{q}}^2 I_2^n(0, 0, \mu_{\tilde{q}}^2) \\
 &\quad + 2(\mu_{\tilde{q}}^2 - \mu_{\tilde{g}}^2) I_2^n(m_{\tilde{q}}^2, 0, \mu_{\tilde{g}}^2) - 2\mu_{\tilde{g}}^2 I_2^n(0, 0, \mu_{\tilde{g}}^2)] \tag{D.6}
 \end{aligned}$$

and the wave function renormalisation constant is

$$\begin{aligned}
 \delta Z_{\tilde{q}} &= \frac{\alpha_s}{4\pi} C_F [4\mu_{\tilde{q}}^2 I_2^n(m_{\tilde{q}}^2, \mu_{\tilde{q}}^2, 0) + 2I_2^n(m_{\tilde{q}}^2, \mu_{\tilde{q}}^2, 0) \\
 &\quad + 2(\mu_{\tilde{g}}^2 - \mu_{\tilde{q}}^2) I_2^n(m_{\tilde{q}}^2, 0, \mu_{\tilde{g}}^2) - 2I_2^n(m_{\tilde{q}}^2, 0, \mu_{\tilde{g}}^2)], \tag{D.7}
 \end{aligned}$$

where the scalar two-point function in  $n = 4 - 2\epsilon$  dimensions is denoted by  $I_2^n$ , defined in the conventions of [89] as

$$\begin{aligned}
 I_2^n(p^2, m_1^2, m_2^2) &= \int \frac{d^n q}{i\pi^{n/2}} \frac{1}{((q+p)^2 - m_1^2 + i\delta)(q^2 - m_2^2 + i\delta)}. \tag{D.8}
 \end{aligned}$$

**References**

1. G. Cullen, N. Greiner, G. Heinrich, G. Luisoni, P. Mastrolia et al., Automated one-loop calculations with GoSam. *Eur. Phys. J. C* **72**, 1889 (2012). [arXiv:1111.2034](#)
2. S. Chatrchyan et al. (CMS Collaboration), Observation of a new boson at a mass of 125 GeV with the CMS experiment at the LHC. *Phys. Lett. B* (2012). [arXiv:1207.7235](#)
3. G. Aad et al. (ATLAS Collaboration), Observation of a new particle in the search for the Standard Model Higgs boson with the ATLAS detector at the LHC. *Phys. Lett. B* **716**, 1–29 (2012). [arXiv:1207.7214](#)
4. S.P. Martin, A Supersymmetry primer. [hep-ph/9709356](#)
5. M.E. Peskin, Supersymmetry in elementary particle physics. [arXiv:0801.1928](#)
6. ATLAS Collaboration, Search for squarks and gluinos with the ATLAS detector using final states with jets and missing transverse momentum and 5.8 fb<sup>-1</sup> of  $\sqrt{s} = 8$  TeV proton–proton collision data. ATLAS-CONF-2012-109

7. G. Aad et al. (ATLAS Collaboration), Search for squarks and gluinos with the ATLAS detector in final states with jets and missing transverse momentum using 4.7 fb<sup>-1</sup> of  $\sqrt{s} = 7$  TeV proton–proton collision data. [arXiv:1208.0949](#)
8. S. Chatrchyan et al. (CMS Collaboration), Search for new physics in the multijet and missing transverse momentum final state in proton–proton collisions at  $\sqrt{s} = 7$  TeV. *Phys. Rev. Lett.* **109**, 171803 (2012). [arXiv:1207.1898](#)
9. B.A. Schumm (ATLAS Collaboration), Searching for supersymmetry with the ATLAS detector at the LHC. ATLAS-PHYS-PROC-2012-134
10. S. Chatrchyan et al. (CMS Collaboration), Search for supersymmetry in hadronic final states using MT2 in  $pp$  collisions at  $\sqrt{s} = 7$  TeV. *J. High Energy Phys.* **1210**, 018 (2012). [arXiv:1207.1798](#)
11. S. Kraml, SUSY status after one year of LHC. [arXiv:1206.6618](#)
12. H.K. Dreiner, J.S. Kim, O. Lebedev, First LHC constraints on neutralinos. *Phys. Lett. B* **715**, 199–202 (2012). [arXiv:1206.3096](#)
13. H.K. Dreiner, S. Heinemeyer, O. Kittel, U. Langenfeld, A.M. Weber et al., Mass bounds on a very light neutralino. *Eur. Phys. J. C* **62**, 547–572 (2009). [arXiv:0901.3485](#)
14. M. Martinez (ATLAS Collaboration), Search for new phenomena in events with a monojet and large missing transverse momentum at the LHC using the ATLAS detector. EPJ Web Conf. **28**, 12015 (2012). [arXiv:1202.0158](#)
15. S. Chatrchyan et al. (CMS Collaboration), Search for dark matter and large extra dimensions in monojet events in  $pp$  collisions at  $\sqrt{s} = 7$  TeV. *J. High Energy Phys.* **1209**, 094 (2012). [arXiv:1206.5663](#)
16. ATLAS Collaboration, Search for dark matter candidates and large extra dimensions in events with a jet and missing transverse momentum with the ATLAS detector. ATLAS-CONF-2012-084
17. ATLAS Collaboration, Search for new phenomena in monojet plus missing transverse momentum final states using 10 fb<sup>-1</sup> of  $pp$  collisions at  $\sqrt{s} = 8$  TeV with the ATLAS detector at the LHC. ATLAS-CONF-2012-147
18. B.C. Allanach, S. Grab, H.E. Haber, Supersymmetric monojets at the large hadron collider. *J. High Energy Phys.* **1101**, 138 (2011). [arXiv:1010.4261](#)
19. M. Drees, M. Hanussek, J.S. Kim, Light stop searches at the LHC with monojet events. *Phys. Rev. D* **86**, 035024 (2012). [arXiv:1201.5714](#)
20. A. Djouadi, A. Falkowski, Y. Mambrini, J. Quevillon, Direct detection of Higgs-portal dark matter at the LHC. [arXiv:1205.3169](#)
21. H.K. Dreiner, M. Kramer, J. Tattersall, How low can SUSY go? Matching, monojets and compressed spectra. *Europhys. Lett.* **99**, 61001 (2012). [arXiv:1207.1613](#)
22. C. Englert, J. Jaeckel, E. Re, M. Spannowsky, Evasive Higgs maneuvers at the LHC. *Phys. Rev. D* **85**, 035008 (2012). [arXiv:1111.1719](#)
23. W. Beenakker, M. Klasen, M. Kramer, T. Plehn, M. Spira et al., The production of charginos/neutralinos and sleptons at hadron colliders. *Phys. Rev. Lett.* **83**, 3780–3783 (1999). [hep-ph/9906298](#)
24. S. AbdusSalam, B. Allanach, H. Dreiner, J. Ellis, U. Ellwanger et al., Benchmark models, planes, lines and points for future SUSY searches at the LHC. *Eur. Phys. J. C* **71**, 1835 (2011). [arXiv:1109.3859](#)
25. M. Kramer, A. Kulesza, R. van der Leeuw, M. Mangano, S. Padhi et al., Supersymmetry production cross sections in  $pp$  collisions at  $\sqrt{s} = 7$  TeV. [arXiv:1206.2892](#)
26. B. Fuks, M. Klasen, D.R. Lamprea, M. Rothering, Gaugino production in proton–proton collisions at a center-of-mass energy of 8 TeV. *J. High Energy Phys.* **1210**, 081 (2012). [arXiv:1207.2159](#)
27. J. Debove, B. Fuks, M. Klasen, Transverse-momentum resummation for gaugino-pair production at hadron colliders. *Phys. Lett. B* **688**, 208–211 (2010). [arXiv:0907.1105](#)

28. J. Debove, B. Fuks, M. Klasen, Joint resummation for gaugino pair production at hadron colliders. *Nucl. Phys. B* **849**, 64–79 (2011). [arXiv:1102.4422](#)
29. J. Debove, B. Fuks, M. Klasen, Threshold resummation for gaugino pair production at hadron colliders. *Nucl. Phys. B* **842**, 51–85 (2011). [arXiv:1005.2909](#)
30. W. Hollik, J.M. Lindert, D. Pagani, NLO corrections to squark-squark production and decay at the LHC. [arXiv:1207.1071](#)
31. W. Beenakker, R. Höpker, M. Spira, P. Zerwas, Squark production at the Tevatron. *Phys. Rev. Lett.* **74**, 2905–2908 (1995). [hep-ph/9412272](#)
32. W. Beenakker, R. Hopker, M. Spira, P. Zerwas, Gluino pair production at the Tevatron. *Z. Phys. C* **69**, 163–166 (1995). [hep-ph/9505416](#)
33. W. Beenakker, R. Höpker, M. Spira, P. Zerwas, Squark and gluino production at hadron colliders. *Nucl. Phys. B* **492**, 51–103 (1997). [hep-ph/9610490](#)
34. G. Bozzi, B. Fuks, M. Klasen, Non-diagonal and mixed squark production at hadron colliders. *Phys. Rev. D* **72**, 035016 (2005). [hep-ph/0507073](#)
35. W. Beenakker, R. Höpker, M. Spira, PROSPINO: a program for the production of supersymmetric particles in next-to-leading order QCD. [hep-ph/9611232](#)
36. S. Bornhauser, M. Drees, H.K. Dreiner, J.S. Kim, Electroweak contributions to squark pair production at the LHC. *Phys. Rev. D* **76**, 095020 (2007). [arXiv:0709.2544](#)
37. W. Hollik, M. Kollar, M.K. Trenkel, Hadronic production of top-squark pairs with electroweak NLO contributions. *J. High Energy Phys.* **0802**, 018 (2008). [arXiv:0712.0287](#)
38. W. Hollik, E. Mirabella, M.K. Trenkel, Electroweak contributions to squark–gluino production at the LHC. *J. High Energy Phys.* **0902**, 002 (2009). [arXiv:0810.1044](#)
39. J. Germer, W. Hollik, E. Mirabella, M.K. Trenkel, Hadronic production of squark–squark pairs: the electroweak contributions. *J. High Energy Phys.* **1008**, 023 (2010). [arXiv:1004.2621](#)
40. J. Germer, W. Hollik, E. Mirabella, Hadronic production of bottom–squark pairs with electroweak contributions. *J. High Energy Phys.* **1105**, 068 (2011). [arXiv:1103.1258](#)
41. W. Beenakker, S. Brensing, M. Kramer, A. Kulesza, E. Laenen et al., Soft-gluon resummation for squark and gluino hadroproduction. *J. High Energy Phys.* **0912**, 041 (2009). [arXiv:0909.4418](#)
42. A. Kulesza, L. Motyka, Threshold resummation for squark–antisquark and gluino-pair production at the LHC. *Phys. Rev. Lett.* **102**, 111802 (2009). [arXiv:0807.2405](#)
43. A. Kulesza, L. Motyka, Soft gluon resummation for the production of gluino–gluino and squark–antisquark pairs at the LHC. *Phys. Rev. D* **80**, 095004 (2009). [arXiv:0905.4749](#)
44. M. Beneke, P. Falgari, C. Schwinn, Threshold resummation for pair production of coloured heavy (s)particles at hadron colliders. *Nucl. Phys. B* **842**, 414–474 (2011). [arXiv:1007.5414](#)
45. P. Falgari, C. Schwinn, C. Wever, NLL soft and Coulomb resummation for squark and gluino production at the LHC. *J. High Energy Phys.* **1206**, 052 (2012). [arXiv:1202.2260](#)
46. M.R. Kauth, J.H. Kuhn, P. Marquard, M. Steinhauser, Gluino pair production at the LHC: the threshold. *Nucl. Phys. B* **857**, 28–64 (2012). [arXiv:1108.0361](#)
47. U. Langenfeld, S.-O. Moch, Higher-order soft corrections to squark hadro-production. *Phys. Lett. B* **675**, 210–221 (2009). [arXiv:0901.0802](#)
48. U. Langenfeld, S.-O. Moch, T. Pfoh, QCD threshold corrections for gluino pair production at hadron colliders. *J. High Energy Phys.* **1211**, 070 (2012). [arXiv:1208.4281](#)
49. D. Goncalves-Netto, D. Lopez-Val, K. Mawatari, T. Plehn, I. Wigmore, Automated squark and gluino production to next-to-leading order. [arXiv:1211.0286](#)
50. D. Goncalves-Netto, D. Lopez-Val, K. Mawatari, T. Plehn, I. Wigmore, Sgluon pair production to next-to-leading order. *Phys. Rev. D* **85**, 114024 (2012). [arXiv:1203.6358](#)
51. T. Binoth, D. Goncalves-Netto, D. Lopez-Val, K. Mawatari, T. Plehn et al., Automized squark–neutralino production to next-to-leading order. *Phys. Rev. D* **84**, 075005 (2011). [arXiv:1108.1250](#)
52. R. Horsky, M. Kramer, A. Mück, P.M. Zerwas, Squark cascade decays to charginos/neutralinos: gluon radiation. *Phys. Rev. D* **78**, 035004 (2008). [arXiv:0803.2603](#)
53. H. Dreiner, M. Kramer, J. Tattersall, Exploring QCD uncertainties when setting limits on compressed SUSY spectra. [arXiv:1211.4981](#)
54. A. Djouadi, J.-L. Kneur, G. Moultaka, SuSpect: a Fortran code for the supersymmetric and Higgs particle spectrum in the MSSM. *Comput. Phys. Commun.* **176**, 426–455 (2007). [hep-ph/0211331](#)
55. C.F. Berger, J.S. Gainer, J.L. Hewett, T.G. Rizzo, Supersymmetry without prejudice. *J. High Energy Phys.* **0902**, 023 (2009). [arXiv:0812.0980](#)
56. T. Binoth, J.-P. Guillet, G. Heinrich, E. Pilon, T. Reiter, Golem95: a numerical program to calculate one-loop tensor integrals with up to six external legs. *Comput. Phys. Commun.* **180**, 2317–2330 (2009). [arXiv:0810.0992](#)
57. G. Cullen, J.P. Guillet, G. Heinrich, T. Kleinschmidt, E. Pilon et al., Golem95C: a library for one-loop integrals with complex masses. *Comput. Phys. Commun.* **182**, 2276–2284 (2011). [arXiv:1101.5595](#)
58. A. van Hameren, OneLoop: for the evaluation of one-loop scalar functions. *Comput. Phys. Commun.* **182**, 2427–2438 (2011). [arXiv:1007.4716](#)
59. T. Stelzer, W. Long, Automatic generation of tree level helicity amplitudes. *Comput. Phys. Commun.* **81**, 357–371 (1994). [hep-ph/9401258](#)
60. R. Frederix, T. Gehrmann, N. Greiner, Automation of the dipole subtraction method in MadGraph/MadEvent. *J. High Energy Phys.* **0809**, 122 (2008). [arXiv:0808.2128](#)
61. R. Frederix, T. Gehrmann, N. Greiner, Integrated dipoles with MadDipole in the MadGraph framework. *J. High Energy Phys.* **1006**, 086 (2010). [arXiv:1004.2905](#)
62. N.D. Christensen, C. Duhr, FeynRules—Feynman rules made easy. *Comput. Phys. Commun.* **180**, 1614–1641 (2009). [arXiv:0806.4194](#)
63. C. Degrande, C. Duhr, B. Fuks, D. Grellscheid, O. Mattelaer et al., UFO—the universal FeynRules output. *Comput. Phys. Commun.* **183**, 1201–1214 (2012). [arXiv:1108.2040](#)
64. P. Mastrolia, G. Ossola, T. Reiter, F. Tramontano, Scattering amplitudes from unitarity-based reduction algorithm at the integrand-level. *J. High Energy Phys.* **1008**, 080 (2010). [arXiv:1006.0710](#)
65. G. Heinrich, G. Ossola, T. Reiter, F. Tramontano, Tensorial reconstruction at the integrand level. *J. High Energy Phys.* **1010**, 105 (2010). [arXiv:1008.2441](#)
66. S. Catani, M. Seymour, A general algorithm for calculating jet cross-sections in NLO QCD. *Nucl. Phys. B* **485**, 291–419 (1997). [hep-ph/9605323](#)
67. Z. Nagy, Z. Trocsanyi, Next-to-leading order calculation of four jet observables in electron positron annihilation. *Phys. Rev. D* **59**, 014020 (1999). [hep-ph/9806317](#)
68. F. Maltoni, T. Stelzer, MadEvent: automatic event generation with MadGraph. *J. High Energy Phys.* **0302**, 027 (2003). [hep-ph/0208156](#)
69. J. Alwall, P. Demin, S. de Visscher, R. Frederix, M. Herquet et al., MadGraph/MadEvent v4: the new web generation. *J. High Energy Phys.* **0709**, 028 (2007). [arXiv:0706.2334](#)
70. S. Frixione, E. Laenen, P. Motylinski, B.R. Webber, C.D. White, Single-top hadroproduction in association with a W boson. *J. High Energy Phys.* **0807**, 029 (2008). [arXiv:0805.3067](#)

71. J.M. Campbell, F. Tramontano, Next-to-leading order corrections to  $Wt$  production and decay. *Nucl. Phys. B* **726**, 109–130 (2005). [hep-ph/0506289](#)
72. O. Buchmueller, R. Cavanaugh, M. Citron, A. De Roeck, M. Dolan et al., The CMSSM and NUHM1 in light of 7 TeV LHC,  $B_s$  to  $\mu^+\mu^-$  and XENON100 data. *Eur. Phys. J. C* **72**, 2243 (2012). [arXiv:1207.7315](#)
73. C. Stenge, G. Bertone, F. Feroz, M. Fornasa, R.R. de Austri et al., Global fits of the cMSSM and NUHM including the LHC Higgs discovery and new XENON100 constraints. [arXiv:1212.2636](#)
74. B. Allanach, SOFTSUSY: a program for calculating supersymmetric spectra. *Comput. Phys. Commun.* **143**, 305–331 (2002). [hep-ph/0104145](#)
75. A. Djouadi, M. Mühlleitner, M. Spira, Decays of supersymmetric particles: the program SUSY-HIT (SUSpect-SdecaY-Hdecay-Interface). *Acta Phys. Pol. B* **38**, 635–644 (2007). [hep-ph/0609292](#)
76. A. Djouadi, J. Kalinowski, M. Spira, HDECAY: a program for Higgs boson decays in the standard model and its supersymmetric extension. *Comput. Phys. Commun.* **108**, 56–74 (1998). [hep-ph/9704448](#)
77. M. Mühlleitner, A. Djouadi, Y. Mambrini, SDECAY: a Fortran code for the decays of the supersymmetric particles in the MSSM. *Comput. Phys. Commun.* **168**, 46–70 (2005). [hep-ph/0311167](#)
78. P.Z. Skands, B. Allanach, H. Baer, C. Balazs, G. Belanger et al., SUSY Les Houches accord: interfacing SUSY spectrum calculators, decay packages, and event generators. *J. High Energy Phys.* **0407**, 036 (2004). [hep-ph/0311123](#)
79. B. Allanach, C. Balazs, G. Belanger, M. Bernhardt, F. Boudjema et al., SUSY Les Houches accord 2. *Comput. Phys. Commun.* **180**, 8–25 (2009). [arXiv:0801.0045](#)
80. T. Hahn, M. Perez-Victoria, Automatized one loop calculations in four-dimensions and D-dimensions. *Comput. Phys. Commun.* **118**, 153–165 (1999). [hep-ph/9807565](#)
81. T. Hahn, Generating Feynman diagrams and amplitudes with FeynArts 3. *Comput. Phys. Commun.* **140**, 418–431 (2001). [hep-ph/0012260](#)
82. T. Hahn, C. Schappacher, The implementation of the minimal supersymmetric standard model in FeynArts and FormCalc. *Comput. Phys. Commun.* **143**, 54–68 (2002). [hep-ph/0105349](#)
83. R.D. Ball, V. Bertone, S. Carrazza, C.S. Deans, L. Del Debbio et al., Parton distributions with LHC data. *Nucl. Phys. B* **867**, 244–289 (2013). [arXiv:1207.1303](#)
84. M. Cacciari, G.P. Salam, G. Soyez, The anti- $k(t)$  jet clustering algorithm. *J. High Energy Phys.* **0804**, 063 (2008). [arXiv:0802.1189](#)
85. M. Cacciari, G.P. Salam, G. Soyez, FastJet user manual. *Eur. Phys. J. C* **72**, 1896 (2012). [arXiv:1111.6097](#)
86. M. Cacciari, G.P. Salam, Dispelling the  $N^3$  myth for the  $k_t$  jet-finder. *Phys. Lett. B* **641**, 57–61 (2006). [hep-ph/0512210](#)
87. B. Allanach, M. Battaglia, G. Blair, M.S. Carena, A. De Roeck et al., The snowmass points and slopes: benchmarks for SUSY searches. *Eur. Phys. J. C* **25**, 113–123 (2002). [hep-ph/0202233](#)
88. A. Denner, S. Dittmaier, M. Roth, Electroweak corrections to charged-current  $e^+e^-$ : 4 fermion processes: technical details and further results. *Nucl. Phys. B* **742** (2005). [hep-ph/0505042](#)
89. T. Binoth, J.P. Guillet, G. Heinrich, E. Pilon, C. Schubert, An algebraic/numerical formalism for one-loop multi-leg amplitudes. *J. High Energy Phys.* **10**, 015 (2005). [hep-ph/0504267](#)